

Small-Scale Compliant Dual Arm with Tail for Winged Aerial Robots

Alejandro Suarez, Manuel Perez, Guillermo Heredia, and Anibal Ollero

Abstract— Winged aerial robots represent an evolution of aerial manipulation robots, replacing the multirotor vehicles by fixed or flapping wing platforms. The development of this morphology is motivated in terms of efficiency, endurance and safety in some inspection operations where multirotor platforms may not be suitable. This paper presents a first prototype of compliant dual arm as preliminary step towards the realization of a winged aerial robot capable of perching and manipulating with the wings folded. The dual arm provides 6 DOF (degrees of freedom) for end effector positioning in a human-like kinematic configuration, with a reach of 25 cm (half-scale w.r.t. the human arm), and 0.2 kg weight. The prototype is built with micro metal gear motors, measuring the joint angles and the deflection with small potentiometers. The paper covers the design, electronics, modeling and control of the arms. Experimental results in test-bench validate the developed prototype and its functionalities, including joint position and torque control, bimanual grasping, the dynamic equilibrium with the tail, and the generation of 3D maps with laser sensors attached at the arms.

I. INTRODUCTION

The use of aerial robots with manipulation capabilities for inspection and maintenance operations in remote or difficult access areas like power lines, solar plants, or pipe structures in chemical plants is justified considering the reduction in time, cost and involved resources, as well as in terms of safety since it contributes to reduce the risk for human operators. Several prototypes of single arm [1]-[4] and dual arm [5][6][7] aerial manipulation robots have been built over multirotor platforms (quadrotors or hexarotors), although other works propose the use of autonomous helicopters [8][9] due to their high payload capacity. However, the vertical take-off and landing (VTOL) platforms like the multirotors and helicopters are not suitable for long endurance or long distance missions since these are not energy efficient for forward flights, but they are intended to hover during the manipulation operation on flight. Note that most works assume that the aerial robot operates on flight, so the aerial platform must support the weight of the manipulator and the interaction forces with the environment. In order to avoid the waste of energy in hovering state, some perching mechanisms have been proposed [10][11][12].

Fixed-wing UAVs are more energy efficient than rotary-wing platforms [13], although they are not capable of flying at low speeds or hovering, whereas flapping-wing aircrafts offer the important advantage of being safer and more efficient in terms of specific power requirement at low speed than rotary-wing UAVs [14]. However, the development of flapping-wing robots (ornithopters) is a research and technological challenge in areas like aerodynamic modelling [15], flight control [16], perching [17], and materials [18]. The ERC Project GRIFFIN [19] aims to develop flapping-wing robots with arms that are

able to perch on a structure and manipulate objects near them. This involves the design and development of new prototypes of robotic arms that are – roughly speaking – one order of magnitude lighter than the arms integrated in multirotors.

In our previous work we developed different prototypes of lightweight [6] and compliant [7] dual arm aerial manipulators in standard (arms placed at the multirotor base) and long reach configuration [20]. These arms were integrated and tested in medium and high scale multirotors, demonstrating bimanual grasping with visual servoing [7], contact force control [21], or inspection operations [20]. The arms were built employing the Herkulex smart servos in two configurations: the classical industrial configuration with three positioning joints [6] (1.8 kg weight, 0.7 kg lift load), and the anthropomorphic dual arm with four positioning joints [7] (1.3 kg, 0.3 kg lift load).

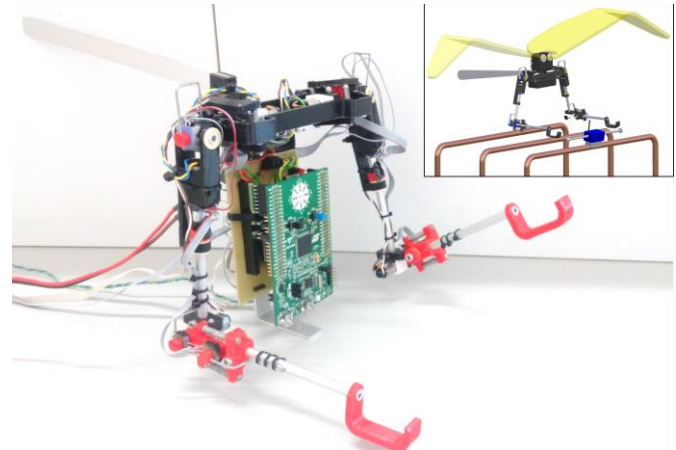


Figure 1. Developed prototype of half-scale compliant dual arm and concept design of winged aerial robot retrieving a small sensor device.

The main contribution of this paper is the design, development and experimental validation of a small-scale dual arm with compliant joints designed for its integration in an ornithopter, that is, a flapping-wing vehicle. A picture of the prototype and the concept design are depicted in Figure 1. The new design requirements and some considerations related to the manufacturing, kinematics, size, and functionalities will be discussed before presenting the developed prototype. This is a 0.2 kg weight, 6-DOF dual arm built using micro-motors and a PLA frame structure that integrates polymer bearings and the position-deflection potentiometers. A compact spring-lever transmission mechanism integrated in the shoulder and elbow joints allow the estimation and control of the torques and forces. The arms are equipped with time-of-flight (ToF) laser sensors that allow the construction of 3D maps of the environment with the motion of the arms. A counterweight tail attached at the back of the shoulder is used to maintain the dynamic equilibrium while perching in cables or branches. Experimental results carried out in a test-bench validate the developed prototype and its functionalities.

Alejandro Suarez (asuarezfm@us.es), Manuel Perez, Guillermo Heredia (guiller@us.es), and Anibal Ollero (aollero@us.es) are with the GRVC Robotics Labs at the University of Seville, Spain.

The rest of the paper is organized in the following way. Section II introduces the design considerations and describes the developed prototype. Section III covers the electronics and low level control of the joint micro-motors, whereas Section IV describes the kinematics, dynamics and control. Section V presents different experimental results that validate the design, summarizing the conclusions in Section VI.

II. HALF-SCALE DUAL ARM DESIGN

A. Description and Specifications

A winged aerial manipulator consists of a fixed or flapping wing aircraft, a manipulator attached at its base and a tail used to control the orientation on flight or in perching situations, as Figure 1 illustrates. Since this kind of aerial platforms is not intended to hover, the payload capacity is lower compared to a multirotor platform. Therefore, special care has to be paid to reduce even more the weight of the manipulator. Roughly speaking, a dual arm manipulator intended for a flapping wing platform should be one order of magnitude lighter (~ 0.2 kg), and half-scale size w.r.t. the human arm (~ 250 mm reach), considering the biomechanical parameters of the pigeons [22] [23]: 0.6 m wingspan, 0.5 kg weight, 0.3 kg lift load.

The prototype presented in this work and shown in Figure 1 is an anthropomorphic compliant dual arm with three actuated joints per arm (shoulder pitch, shoulder yaw and elbow pitch). The shoulder roll joint is non-actuated, although its rotation angle can be preset manually. The arms are built with Pololu micro metal gear motors (250:1, 10 g weight, 3.7 kg·cm stall torque), and a customized 3D printed PLA frame structure with aluminum shafts, measuring the rotation and deflection angles with Murata SV01 potentiometers. The rotation of the joints is supported by sixteen polymer flange bearings JFM-0608-04 manufactured by igus. The mass and inertia of the different parts of the dual arm are represented in Table 1 and Figure 2, whereas Table 2 contains the mass density and total mass of the materials employed.

Table 1. Mass and inertia parameters of the small-scale compliant dual arm.

	Mass [g]	I_{xx} [g·cm ²]	I_{yy} [g·cm ²]	I_{zz} [g·cm ²]
Sh. Pitch	36	52	478	496
Sh. Roll	19	59	30	57
Sh. Yaw	19	42	47	9
E. Pitch	19	110	105	13
Forearm	20	387	392	20

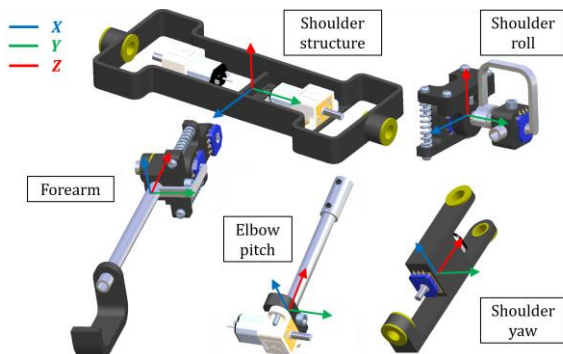


Figure 2. Rendered view with the different parts of the small scale dual arm. The coordinate axes are placed at the center of mass of each link (Table 1).

Table 2. Mass density (g/cm³) of the different components used in the arms.

Material	PLA	Polymer	Alum.	Motors	Steel
Component	Frame struct.	Flange bearings	Shafts, links	Micro-motors	Screws, nuts, springs
M. density	1.2	1.24	2.7	3.0	7.8
Total mass	60	3	21	60	24
Num. parts	25	16	16	6	60

It is interesting to compare Table 1 with the parameters of the compliant dual arm described in [7], resulting significant the reduction in the number of parts as the scale is smaller. The total weight of the arms, excluding the microcontroller board, is around 0.2 kg, that is, six times lighter than [7]. Note however that in this prototype the shoulder roll joint is not actuated to reduce the weight and simplify the mechanics. The anthropomorphic configuration is adopted since the design of the shoulder structure and the integration of the spring-lever transmission mechanism is more compact compared to [6]. It is also assumed that the manipulation operation is carried out once the aerial robot has landed and the wings are folded.

B. Compliant Joint Transmission

The half-scale compliant dual arm integrates a spring-lever transmission mechanism in the shoulder pitch and elbow pitch joints [7], allowing the estimation and control of the torques and forces from the deflection measurement [21] (see Section IV-C). Although the torque delivered by a DC motor can be controlled through the current, the accuracy and sensitivity at the output shaft of the gearbox will be low. The introduction of an elastic element between the motor shaft and the output link also contributes to increase safety in those tasks involving physical interaction, and protects the gearbox against impacts. The mechanism implemented in these two joints is detailed in Figure 3 and Figure 4. The rotation of the spring-lever in the shoulder pitch joint is supported by a pair of igus JFM-0608-04 polymer bearings fitted side-by-side into the PLA frame of the shoulder structure. Due to space limitations, the rotation angle of the upper arm link is measured with a Murata SV01A potentiometer attached to the shoulder roll structure, rotating the wiper with a rigid wire connected to the shoulder frame. The deflection potentiometer is placed between the two plastic levers, as Figure 3 illustrates.

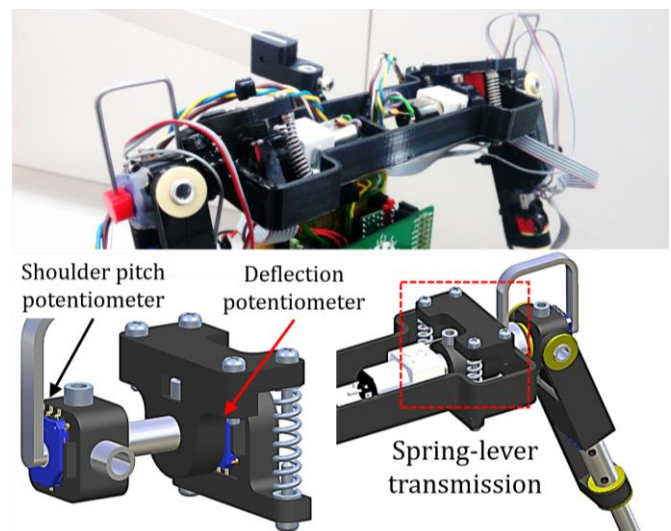


Figure 3. Detailed view of the compliant shoulder pitch joint.

The design of the compliant elbow joint introduces a slight modification so the compliant transmission is more compact. As it can be seen in Figure 4, the spring-lever mechanism is rigidly attached to the shaft of the elbow motor, whereas the forearm link rotates with respect to a parallel joint displaced 25 mm from the motor shaft. Two potentiometers mounted on the plastic frame of the forearm structure measure the rotation angle of the elbow micro motor and the deflection angle in the passive compliant joint. Although this modifies the kinematics of the manipulator, its effect in practice is relatively low due to the proximity with the elbow axis.

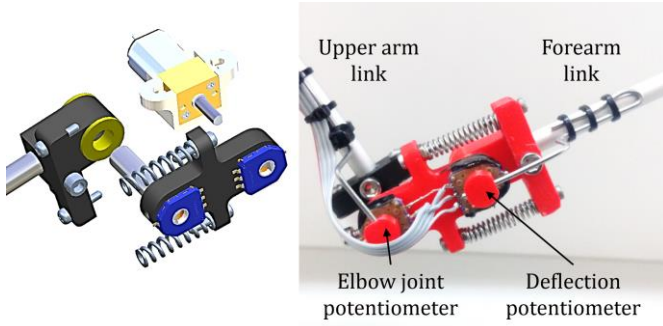


Figure 4. Detailed view of the elbow joint with compliant passive joint.

C. Tail Mechanism

The winged aerial robot is intended to conduct inspection operations while perching in cables of power lines or in pipe structures in chemical plants, so it is necessary to ensure that the body maintains the equilibrium despite the variation of the center of mass caused by the movement of the arms. For this purpose, the prototype presented here includes a 25 cm length aluminium tail actuated by another motor in the pitch angle, integrating an inertial measurement unit (IMU) to measure the orientation and control the tail angle to maintain the dynamic equilibrium. Figure 5 depicts the setup, showing some results in Section V-D. Although in this work the tail is used simply as counterweight, it is expected to extend its surface to control the attitude of the flapping-wing platform during the flight.

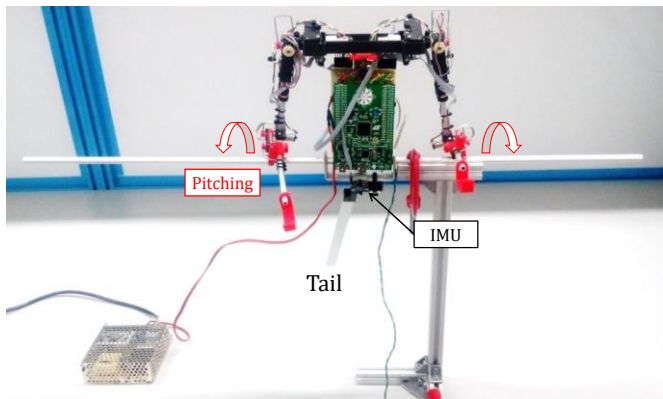


Figure 5. Dynamic equilibrium emulating perching condition, using the tail to compensate the pitching angle measured by the IMU.

III. ELECTRONICS

Unlike our previous dual arm prototypes [6][7], built with the Herkulex smart servos, the small-scale compliant dual arm employs Pololu micro metal gear motors 250:1 HP (10 grams weight, 3.7 kg·cm stall torque, 120 RPM @ 6V), requiring a

customized electronics for controlling the position, velocity or torque. Figure 6 depicts the components and their distribution according to the kinematic configuration described in Section IV (Figure 7). The robot consists of seven micro-motors, three for each of the arms, and one for the tail, used to maintain the equilibrium in perching conditions. Three types of angles are measured with the Murata SV01 potentiometers: 1) deflection angle in the shoulder and elbow pitch joints, 2) micro-motor shaft rotation angle in the elbow pitch joint, and 3) output link rotation angle (shoulder pitch). As described in Section IV-C, the torque in the compliant joints is estimated from the deflection angle, allowing the control of the torques and forces [21]. A STM32F3 Discovery microcontroller board is used to read the analog signals from the potentiometers and generate the PWM (Pulse Width Modulation) signals applied to the micro-motor drivers to control the current/speed. Additionally, the system integrates two VL53L1X-SATEL time-of-flight distance sensors used to generate a map with the obstacles in the environment (see experiment in Section V-E).

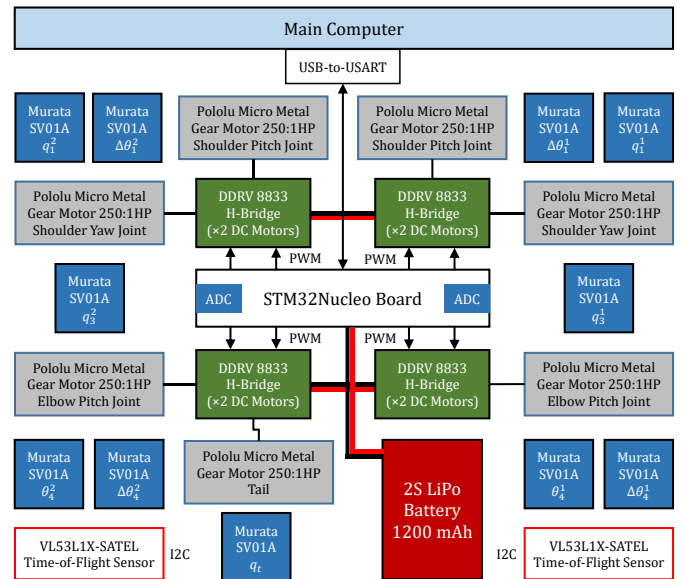


Figure 6. Electronic components of the small-scale compliant dual arm.

Four DRV8833 drivers are used to control the six micro motors of the arms and the additional motor of the tail. Due to the inductive nature of brushed motors, the current must keep flowing when the windings are not fed. The DRV8833 driver provides two operation modes depending on the way that the recirculation of the current is achieved: 1) fast decay mode, in which the current flows through the diodes of the MOSFET transistor, or 2) slow decay mode in which the terminals of the motor are short-circuited. Experimental tests evidence that the second mode is more convenient as the electric brake reduces the current consumption when the arms have to stay in a static position with a certain load, and because the performance of the position controller is better, as evaluated in Section V-C. The slow decay mode requires two PWM signals per motor (14 in total) to control the rotational speed and direction. The frequency of the PWM signal is set to 15 kHz to avoid that the brushes of the DC motors produce an annoying buzz. The software of the STM32F3 Discovery board was developed in C/C++ using the Atollic TrueSTUDIO IDE, the STM32Cube tool, and the Hardware Abstraction Layer (HAL) library. The update rate of the main control loop is set to 100 Hz.

IV. MODELLING AND CONTROL

A. Kinematics

The small-scale compliant dual arm implements the human-like kinematic configuration described in [7], with four joints for end-effector positioning: shoulder pitch, roll and yaw, and elbow pitch. However, in the new prototype, the shoulder roll joint is not actuated, but its rotation angle is pre-set to reduce the weight and simplify the mechanics, and because in most bimanual manipulation tasks the arms operate in the forward direction, so this angle does not vary significantly.

The joint angles, link lengths, reference frames and position vectors of the manipulator are depicted in Figure 7. In the following, superscript $i = \{1, 2\}$ will denote the left or right arm, whereas subscript $j = \{1, 2, 3, 4\}$ will represent the joint index in the order indicated before. In this way, q_j^i represents the rotation angle of the j -th joint of the i -th arm. For clarity and coherence in the notation, we assume that the rotation angle of the shoulder roll joint is fixed and known, $q_2^i = \varphi^i$. The rotation angle of the micro-motor shaft is denoted by θ_j^i , defining the deflection angle of the compliant joint, $\Delta\theta_j^i$, as the difference between the motor shaft and the output link rotation angle:

$$\Delta\theta_j^i = \theta_j^i - q_j^i \quad (1)$$

Note that for a stiff joint $\theta_j^i = q_j^i$ and thus $\Delta\theta_j^i = 0$.

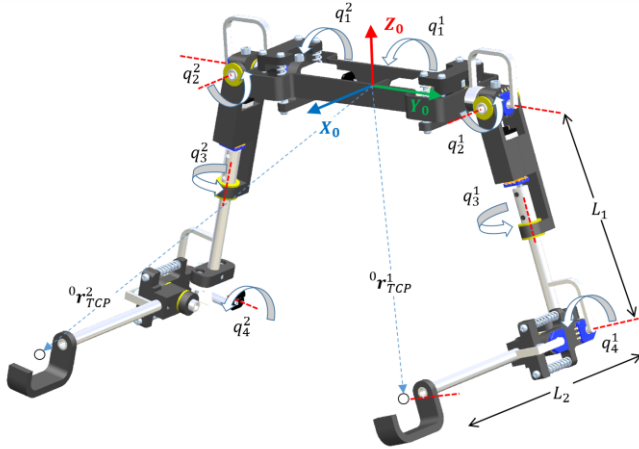


Figure 7. Kinematic model of the small scale dual arm in anthropomorphic configuration: reference frame, lengths, joint angles and position vectors.

The resolution of the forward and inverse kinematics can be found in ref. [7]. The concepts of Cartesian deflection and virtual variable impedance control developed in [21] can be applied to this prototype as the kinematics is the same.

B. Dynamic Model

The dynamics of the small-scale compliant dual arm can be derived from the Lagrangian and the generalized equation of the forces and torques expressed as:

$$\frac{d}{dt} \left\{ \frac{\partial L}{\partial \dot{\mathbf{q}}} \right\} - \frac{\partial L}{\partial \mathbf{q}} = \mathbf{\Gamma} \quad (2)$$

$$L = K - V \quad (3)$$

where L is the Lagrangian, K and V are the kinetic and potential energy, respectively, whereas \mathbf{q} and $\mathbf{\Gamma}$ are the vectors of generalized coordinates and forces, given by:

$$\mathbf{q} = [\boldsymbol{\theta}^{1,T} \quad \boldsymbol{\theta}^{2,T} \quad \mathbf{q}^{1,T} \quad \mathbf{q}^{2,T} \quad q_{tail}]^T \in \mathbb{R}^{12} \quad (4)$$

$$\mathbf{\Gamma} = [\boldsymbol{\tau}_m^{1,T} \quad \boldsymbol{\tau}_m^{2,T} \quad \boldsymbol{\tau}^{1,T} \quad \boldsymbol{\tau}^{2,T} \quad \tau_{tail}]^T \in \mathbb{R}^{12} \quad (5)$$

where $\boldsymbol{\theta}^1$ and $\boldsymbol{\theta}^2$ are the joint position vectors referred to the motor shaft of the left and right arms, \mathbf{q}^1 and \mathbf{q}^2 are the corresponding output link rotation angles, whereas q_{tail} is the rotation angle of the tail. As stated in [21], the dynamic model of a compliant joint manipulator can be expressed in the usual matrix form:

$$\mathbf{M}(\mathbf{q})\ddot{\mathbf{q}} + \mathbf{C}(\mathbf{q}, \dot{\mathbf{q}}) + \mathbf{G}(\mathbf{q}) + \mathbf{K}(\mathbf{q}) + \mathbf{D}(\mathbf{q}) = \mathbf{\Gamma} \quad (6)$$

where \mathbf{M} is the generalized inertia matrix, \mathbf{C} represents the Coriolis and centrifugal terms, \mathbf{G} and \mathbf{K} are gravity and elastic potential terms, and \mathbf{D} corresponds to the damping term.

C. Micro-Motor Control

The developed small-scale compliant dual arm implements three control modes at joint level: open-loop velocity control (PWM), closed loop position control, and closed-loop torque control based on deflection measurement. In the design of the controller it is assumed that the motor dynamics is given by:

$$J\ddot{\theta} + f\dot{\theta} + \text{sign}(\dot{\theta})\tau_{fc} = k \cdot \text{pwm} \quad (7)$$

where J and f are the inertia and friction of the micro-motor shaft, τ_{fc} is the Coulomb friction, $\text{pwm} \in [-1, 1]$ represents the PWM signal, whereas k is the PWM-torque constant. The angular velocity of the micro motor can be regulated directly through the PWM signal, neglecting the inertial term in Eq. (7). Note that the angular acceleration is usually too noisy to estimate this term from the measurement of the potentiometer.

A Proportional-Integral (PI) controller is executed at 100 Hz in the microcontroller board to control the joint position through the PWM signal applied to the H-bridge (Figure 6):

$$\text{pwm}_\theta = \begin{cases} PWM_{max} & \text{if } |\theta_\varepsilon| \geq \theta_\varepsilon^{th} \\ K_{P,\theta}\theta_\varepsilon + K_{I,\theta} \int \theta_\varepsilon dt & \text{if } |\theta_\varepsilon| < \theta_\varepsilon^{th} \end{cases} \quad (8)$$

Here $\theta_\varepsilon = \theta_{ref} - \theta$ is the joint position error, and $K_{P,\theta}$ and $K_{I,\theta}$ are proportional and integral gains of the controller. The term PWM_{max} limits the rotation speed of the motor when the error is above the threshold θ_ε^{th} , avoiding the wind-up effect.

The torque controller is implemented in a similar way to the position controller, considering the torque error instead:

$$\text{pwm}_\tau = K_{P,\tau} \cdot \tau_\varepsilon + K_{I,\tau} \cdot \int \tau_\varepsilon dt \quad (9)$$

where $K_{P,\tau}$ and $K_{I,\tau}$ are the proportional and integral gains, and τ_ε is the torque error estimated from the joint deflection in Eq. (1), and the joint stiffness k and damping d [21]:

$$\tau_\varepsilon = \tau_{ref} - (k \cdot \Delta\theta + d \cdot \dot{\Delta}\theta) \quad (10)$$

The gains of the controllers were tuned empirically, taking into account that $\theta_\varepsilon \sim 10^\circ$, and a torque error $\tau_\varepsilon \sim 0.1 \text{ Nm}$. These controllers will be evaluated in Section V-C.

V. EXPERIMENTAL RESULTS

A. Frequency Identification

The goal of this experiment is to identify the bandwidth of the Pololu micro metal gear motors employed in the small scale dual arm prototype as well as the resonance peaks in the deflection signal measured by the potentiometers integrated in the shoulder pitch and in the elbow pitch joints, according to Figure 3 and Figure 4. For this purpose, the DC motors are excited with a sine chirp signal applied over the PWM signal given by:

$$pwm_j^{1,2} = PWM_{max} \cdot \sin\left(\frac{f_{max} \cdot \pi \cdot t}{T_{scan}} \cdot t\right) \quad (11)$$

where $PWM_{max} = 50\%$ of the duty cycle, $f_{max} = 5 \text{ Hz}$, and $T_{scan} = 60$ seconds. The shoulder and elbow pitch joints of both arms are excited separately, representing in Figure 8 the module of the Fast Fourier Transform (FFT) of the four signals of interest: PWM reference, shoulder-elbow angular position, and shoulder-elbow joint deflection. It is interesting to compare these results with the frequency analysis shown in [7], where the resonance peaks in the deflection signal were more evident. In this prototype, however, the mass and inertia are significantly smaller, and the damping effect also reduces the amplitude of the deflection. Figure 8 also reveals that the 3 dB bandwidth of the DC micro motors is around 1 Hz.

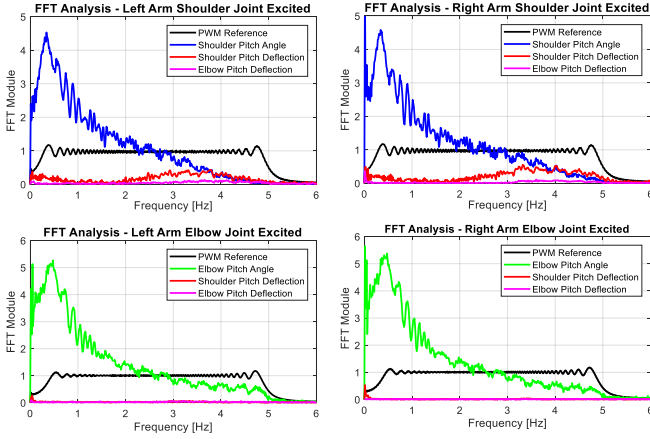


Figure 8. Frequency response of the shoulder pitch (blue) and elbow pitch (green) joints and corresponding deflection (red, magenta) for a sine chirp signal in the range 0 – 5 Hz and a 50% duty cycle.

B. Bimanual Teleoperation for Bar Retrieval

In this experiment, both left and right arms are controlled in PWM mode (Section IV-C) using a single 3DConnexion Space Navigator mouse. The task consists of retrieving a bar placed in a tool bench at 10 cm in front of the arms. The operator commands directly the PWM signal given to the shoulder pitch, shoulder yaw, and elbow pitch micro-motors through the Δx , $\Delta \psi$, and Δz inputs of the mouse, respectively. Figure 9 represents the 3D trajectory followed by the TCP of both arms along with the evolution of the joint trajectories. The arms start from the initial pose $q_1 = 60$, $q_2 = 0$, $q_3 = 0$, and $q_4 = -90$ deg, moving in the forward direction (X-axis) until $t = 8$, when the operator rotates the shoulder yaw joint to approach the end effector to the tool, which is retrieved at $t = 11$ s, moving the arms backwards.

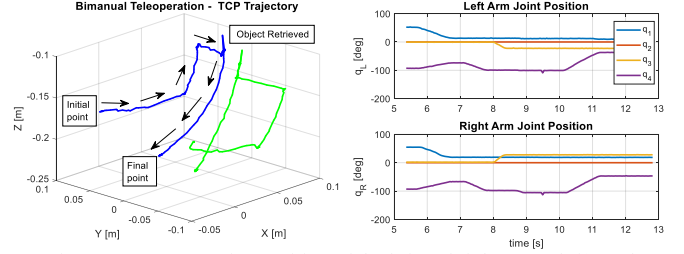


Figure 9. TCP Cartesian position of the left and right arms (left), and evolution of the joint variables (right).

C. Joint Position and Torque Control

The performance of the joint position and torque controllers described in Section IV-C are evaluated here, generating the sequence of references depicted in Figure 10 and Figure 11. In both cases, the PWM signal applied to the motor driver is computed from the joint position or deflection signal given by the analog potentiometers. The performance of the joint position controller is better since it is executed in the micro-controller board at 100 Hz, whereas the torque controller is implemented in a computer board, sending the feedback and the references through the USART interface at 50 Hz. The experimental results evidence the convenience of using high accuracy digital encoders to measure the angular position and the deflection signal instead of analog sensors more affected by noise. The deflection of the joints during the execution of the torque control task is illustrated in the attached video.

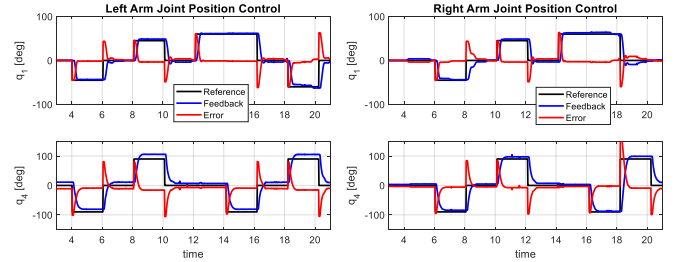


Figure 10. Sequence of position references applied to the shoulder and elbow pitch joints of the left and right arms.

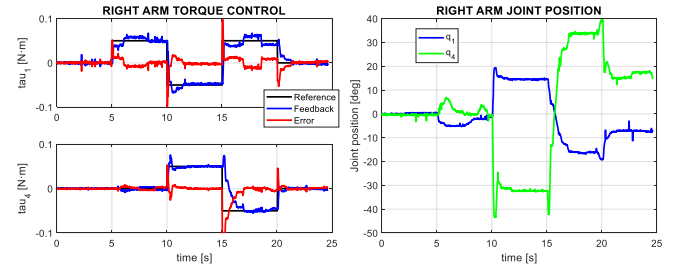


Figure 11. Sequence of torque references applied to the shoulder and elbow pitch joints of the right arm (left), and joints position (right).

D. Dynamic Equilibrium with Tail while Perching

As stated in the introduction, this first prototype of a small-scale dual arm was designed for its integration in a flapping wing aerial platform capable of perching in wrenches or cables, in a similar way birds do. For this purpose, the dual arm is equipped with a 25 cm tail that helps the manipulator to maintain the equilibrium in perching conditions, as Figure

5 depicted. The integrated IMU is used to measure the body orientation, controlling the pitch angle through the rotation angle of the tail. Figure 12 represents the Euler XYZ angles of the robot along with the rotation angle of the tail and the joint angles of the arms when these are moved manually forwards-backwards using the 3DConnexion mouse. A PID controller tuned empirically generates the PWM signal of the tail micro-motor that tends to cancel the oscillation in pitch measured by the IMU. The oscillation between $t = 4$ and $t = 6.5$ seconds is mainly due to the clearance of the micro motor (around 3 deg) and the noise in the measured angle. Figure 13 shows a sequence of images taken from the attached video illustrating the bimanual grasping of a bar using the tail to maintain the equilibrium.

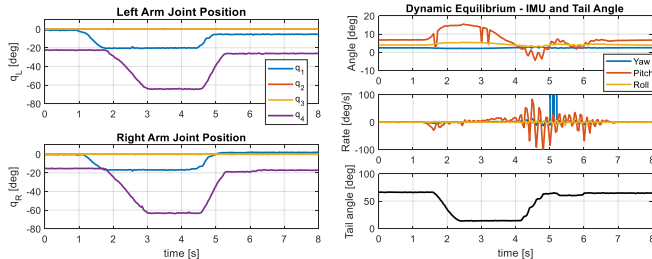


Figure 12. Left and right arms joint position (left), orientation, angular rate and tail angle (right).

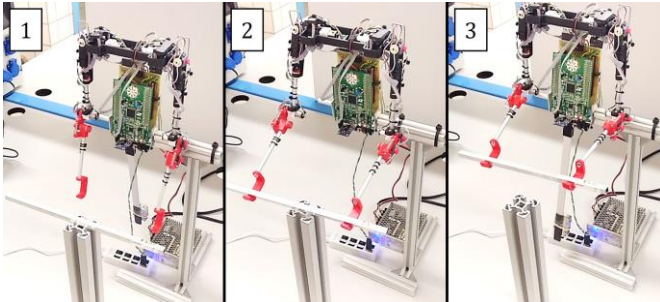


Figure 13. Bimanual grasping of a bar emulating perching conditions using the tail as counterweight to maintain the dynamic equilibrium.

E. Generation of Obstacle Maps using Laser Sensors

The dual arm system incorporates two VL53L1X-SATEL Time-of-Flight (ToF) sensors, attached at the end effector of both arms to measure the distance to close obstacles along the direction of the forearm link. Generating a scan trajectory with the dual arm, and adding the measured distance to the forearm link length in the forward kinematic model [7], it is possible to obtain a point cloud that represents a map of the environmental obstacles w.r.t the manipulator frame. This data may be useful for navigation and motion planning in narrow spaces. Figure 14 shows the point cloud generated in the scenario depicted below, consisting of a flat wall and two vertical bars of 40×40 mm size. In the execution of the experiment, the left arm is focused permanently on Obstacle #1 while the right arm performs a scan rotating the shoulder yaw joint. As it can be seen, the accuracy in the detection of the obstacles with the second arm is lower due to the 25° view cone of the laser receptor and because of the errors in the measurement of the joint angles.

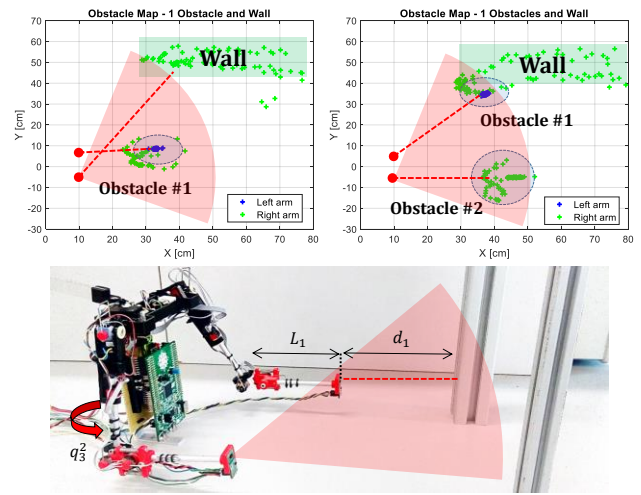


Figure 14. XY-axes obstacle maps with one (up, left) and two (up, right) obstacles and the wall. Experimental setup (down).

VI. CONCLUSION AND FUTURE WORK

This paper has presented a first prototype of small-scale compliant dual arm designed for its integration in a fixed or flapping wing aerial robot, where the payload constraints are even stronger than with multirotor platforms. The proposed prototype provides 6-DOF's for end effector positioning in a human-like kinematic configuration, with a reach of 250 mm, 0.2 kg weight, and around 0.1 kg payload per arm. Unlike our previous dual arm prototypes [6][7], built the Herkulex smart servos (45–150 g weight, 1.2–7.0 N·m torque), the prototype described in this paper is built with Pololu micro metal gear motors due to their low weight (10 g), relatively high torque (~ 0.2 N·m), and low cost (18 \$). A customized electronics was developed to measure and control the joint position and torque, implementing the low-level control of the motors.

In this work, it is assumed that the manipulation operation is carried out once the aerial robot has landed or is perching. The integration of the arms in the flapping-wing platform has to be analyzed carefully considering the mass distribution of the compound, as well as the aerodynamic effect of the arms during the flight.

As future work, it is necessary to simplify the assembly process and reduce the wiring drastically. In this sense, one solution of special interest is the development of small smart servos integrating the actuator, electronics and control in a compact device, with a weight around 20 g, and allowing the connection of multiple devices through a common bus (V_{cc} , GND and Rx/Tx). The use of new materials, structures, and manufacturing methodologies is also essential to improve the quality and performance of this new kind of robotic arms.

ACKNOWLEDGEMENT

This work has been funded by the European Research Council Advanced Grant GRIFFIN (General compliant aerial Robotic manipulation system Integrating Fixed and Flapping wings to INcrease range and safety), Action 788247, and the

ARM-EXTEND (DPI2017-89790-R) and ARTIC (RTI2018-102224-B-I00) projects, funded by the Spanish Ministerio de Economía, Industria, y Competitividad.

- [22] T. Bachmann, "Anatomical, morphometrical and biomechanical studies of barn owls and pigeons' wings," in RTWH Aachen University, 2011.
 [23] J. H. Marden, "Maximum lift production during takeoff in flying animals," in *Journal of Experimental Biology*, 130 (1), 235–258.

REFERENCES

- [1] S. Kim, H. Seo and H. J. Kim, "Operating an unknown drawer using an aerial manipulator," in *IEEE International Conference on Robotics and Automation (ICRA)*, May 2015, pp. 5503–5508.
 [2] F. Ruggiero *et al.*, "A multilayer control for multirotor UAVs equipped with a servo robot arm," *IEEE International Conference on Robotics and Automation (ICRA)*, Seattle, WA, 2015, pp. 4014–4020.
 [3] C. D. Bellicoso, L. R. Buonocore, V. Lippiello and B. Siciliano, "Design, modeling and control of a 5-DoF light-weight robot arm for aerial manipulation," *2015 23rd Mediterranean Conference on Control and Automation (MED)*, Torremolinos, 2015, pp. 853–858.
 [4] A. Suarez, G. Heredia and A. Ollero, "Lightweight compliant arm with compliant finger for aerial manipulation and inspection," in *2016 IEEE/RSJ International Conference on Intelligent Robots and Systems (IROS)*, Daejeon, 2016, pp. 4449–4454.
 [5] M. Orsag, C. Korpela, S. Bogdan and P. Oh, "Dexterous aerial robots - mobile manipulation using unmanned aerial systems," in *IEEE Transactions on Robotics*, vol. 33, no. 6, 2017, pp. 1453–1466.
 [6] A. Suarez, A. E. Jimenez-Cano, V. Vega, G. Heredia, A. Rodriguez-Castaño, and A. Ollero, "Design of a lightweight dual arm system for aerial manipulation," in *Mechatronics*, Vol. 50, 2018, pp. 30–44.
 [7] A. Suarez, G. Heredia and A. Ollero, "Design of an anthropomorphic, compliant, and lightweight dual arm for aerial manipulation," in *IEEE Access*, vol. 6, 2018, pp. 29173–29189.
 [8] K. Kondak, F. Huber, M. Schwarzbach, M. Laiacker, D. Sommer, M. Bejar, and A. Ollero, "Aerial manipulation robot composed of an autonomous helicopter and a 7 degrees of freedom industrial manipulator," *2014 IEEE International Conference on Robotics and Automation (ICRA)*, Hong Kong, 2014, pp. 2107–2112.
 [9] P. E. Pounds, D. E. Bersak, A. M. Dollar, "The yale aerial manipulator: grasping in flight," in *IEEE International Conference on Robotics and Automation*, 2011, pp. 2974–2975.
 [10] V. Ghadiok, J. Goldin, W. Ren, "Autonomous indoor aerial gripping using a quadrotor," *IEEE/RSJ International Conference on Intelligent Robots and Systems*, San Francisco, CA, 2011, pp. 4645–4651.
 [11] C. E. Doyle *et al.*, "An avian-inspired passive mechanism for quadrotor perching," in *IEEE/ASME Transactions on Mechatronics*, vol. 18, no. 2, 2013, pp. 506–517.
 [12] H. Paul, K. Ono, R. Ladig, and K. Shimonomura, "A multirotor platform employing a three-axis vertical articulated robotic arm for aerial manipulation tasks," in *IEEE/ASME International Conference on Advanced Intelligent Mechatronics*, Auckland, 2018, pp. 478–485.
 [13] R. Beard, D. Kingston, M. Quigley, D. Snyder, R. Christiansen, W. Johnson, T. McLain, M. Goodrich, "Autonomous vehicle technologies for small fixed-wing UAVs", in *Journal of Aerospace Computing, Information, and Communication*, Vol. 2, No. 1, 2005, pp. 92–108.
 [14] M.I. Woods, J.F. Henderson and G.D. Lock, "Energy requirements for the flight of micro air vehicles," *Aeronaut. J.*, 105, 2001, pp. 135–149.
 [15] M. Platzer, K. Jones, J. Young, J. Lai, "Flapping wing aerodynamics: progress and challenges," *Aiaa Journal - AIAA J.* 46. 2008, 2136–2149.
 [16] P. Chirarattananon, K. Ma, Kevin, and R. Wood, "Adaptive control of a millimeter-scale flapping-wing robot," *Bioinspiration & Bio-mimetics*. Vol. 9(2), 2018, 025004.
 [17] A. A. Paranjape; S.J. Chung, J.Kim, "Novel dihedral-based control of flapping-wing aircraft with application to perching," *IEEE Transactions on Robotics*, vol. 29, 5, 2013, pp. 1071–1084.
 [18] L. Hines, V. Arabagi and M. Sitti, "Shape memory polymer-based flexure stiffness control in a miniature flapping-wing robot," in *IEEE Transactions on Robotics*, vol. 28, no. 4, 2012, pp. 987–990.
 [19] GRIFFIN ERC Advanced Grant Project, <https://griffin-erc-advanced-grant.eu/>
 [20] A. Suarez, P. Sanchez-Cuevas, M. Fernandez, M. Perez, G. Heredia, A. Ollero, "Lightweight and compliant long reach aerial manipulator for inspection operations," *2018 IEEE/RSJ International Conference on Intelligent Robots and Systems (IROS)*, Madrid, 2018, pp. 6746–6752.
 [21] A. Suarez, G. Heredia and A. Ollero, "Physical-virtual impedance control in ultra-lightweight and compliant dual-arm aerial manipulators," in *IEEE Robotics and Automation Letters*, vol. 3, no. 3, 2018, pp. 2553–2560.